

Potential to Estimate the Canting Angle of Tilted Structure in Clouds from Microwave Radiances around 183 GHz

Gang Hong, Georg Heygster, *Member, IEEE*, Jungang Miao, and Klaus Kunzi, *Senior Member, IEEE*

Abstract—The effects of cloud structures on microwave radiances at frequencies from 89 to 190 GHz are investigated by simulations using the Goddard Cumulus Ensemble (GCE) model data as input for a radiative transfer model. It was found that the brightness temperatures at these frequencies have different sensitivities to clouds with a tilted structure. The different sensitivities to altitude and amount of hydrometeors allow to estimate the canting angle and tilt direction of tilted cloud using brightness temperatures at the water vapor channels at 183.3 ± 1 and 183.3 ± 7 GHz. The estimated canting angle and tilt direction are in agreement with the model situation. This method provides a potential to estimate tilted convective structures from microwave radiometric observations at 183.3 ± 1 and 183.3 ± 7 GHz. It is applied to a tilted storm observed from the NASA ER-2 aircraft flying at about 20 km on 26 August 1998 during the Convection And Moisture EXperiment (CAMEX)-3 using the observed down-looking brightness temperatures at the water vapor channels of a Millimeter-wave Imaging Radiometer (MIR). The estimated results are in good agreement with the realistic storm situation obtained from the simultaneous observations of the ER-2 Doppler radar (EDOP). This method also provides information about the vertical displacement of cloud structure and thereby to estimate the accurate location of surface rainfall. This is important when validating precipitation retrieval based on observations of the ice scattering above surface rainfall against surface rain observations using the microwave frequencies sensitive to high altitudes.

Index Terms—Microwave radiance, water vapor channel, tilted cloud, canting angle.

I. INTRODUCTION

The Advanced Microwave Sounding Unit (AMSU)-B onboard the NOAA-15, 16 and 17 satellites is primarily designed to measure radiation from a number of different layers of the atmosphere in order to obtain global data on humidity profiles (e.g., [1]). The key advantage of the AMSU-B channels with frequencies between 89 and 190 GHz is the unique ability to penetrate clouds (e.g., [2] and [3]). However, the atmosphere is not entirely transparent at these frequencies in cases where thick clouds or precipitation significantly contaminate the sounder's field of view [4]. Consequently, the effects of cloud and precipitation on brightness temperatures provide possibilities to estimate cloud parameters, especially at the AMSU-B window channels (89 and 150 GHz) [5]–[7].

Several simulations (e.g., [2] and [8]–[10]) and aircraft observational studies (e.g., [11] and [12]) have examined the

effects of clouds on microwave radiances at the frequencies between 89 and 190 GHz. The presence of hydrometeors in the upper levels of cloud with high cloud top result in large brightness temperature depressions at these frequencies above 150 GHz. Furthermore, for three channels (183.3 ± 1 , 183.3 ± 3 , and 183.3 ± 7 GHz) around the water vapor absorption line centered at 183.3 GHz, the farther the frequency is from the center, the larger is the brightness temperature depression [2]. This is because the 183.3 ± 7 GHz channel can view deeper into clouds than the other two water vapor channels. The temperature weighting functions of the three water vapor channels peak at different altitudes, and they are above 9 km for precipitating clouds [2]. Their different altitude responses entail a potential to delineate the distribution of hydrometeors in clouds [2], [11], [13].

Making use of the correlation between ice scattering and surface rain rate [5], the frequencies between 89 and 190 GHz are able to delineate precipitation (e.g., [7]). Staelin and Chen [14] used for the first time the 183.3 ± 1 and 183.3 ± 7 GHz channels to estimate precipitation. The physical basis of their retrieval is that hydrometeors reduce the brightness temperature below the frequency-dependent value for a saturated atmosphere. However, convective systems are not always exactly vertical, many of them are tilted (Fig. 1) (e.g., [15]–[17]). The ice particles aloft shift horizontally away from heavy surface rainfall regions because the convective cores and rain shafts are tilted (e.g., [16], [17]). Therefore, the rain retrieval methods based on the correlation between ice scattering and the surface rain rate provide a displacement of cloud ice and surface rain, which was discussed for lower frequencies at 19 and 85 GHz by Hong and Haferman [17].

In this study, hydrometeor profiles of a tropical squall line system from the Goddard Cumulus Ensemble (GCE) model output are used as input for a microwave radiative transfer model. The simulated brightness temperatures at 89–190 GHz are used to investigate the effects of cloud structures on brightness temperatures. Different characteristics due to different sensitivities to altitude and amount of hydrometeors in a tilted cloud suggest a method to estimate the canting angle and tilt direction of the cloud from brightness temperatures at water vapor channels centered around 183 GHz. This method is also applied to a tilted storm observed by simultaneous aircraft microwave and radar data. The knowledge of the canting angle provides the possibility to estimate the accurate location of surface rainfall when retrieving it from the ice scattering above surface rainfall.

G. Hong, G. Heygster, and K. Kunzi are with the Institute of Environmental Physics, University of Bremen, Post Box 330440, Bremen 28203, Germany. (honggang@uni-bremen.de)

J. Miao is with the Electromagnetics Laboratory, Baihang University, Beijing 100083, China.

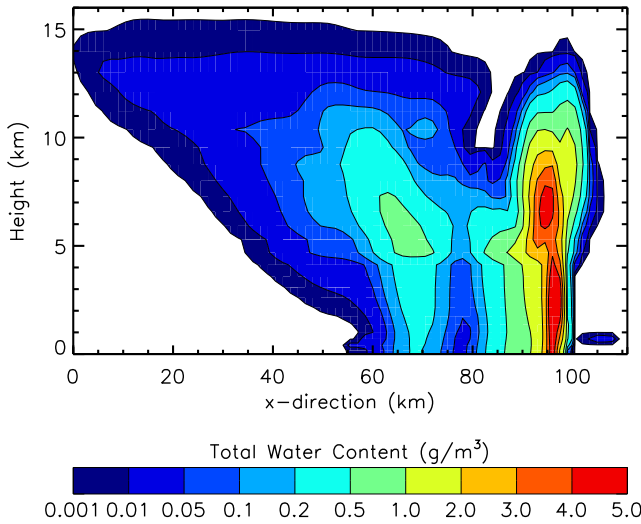


Fig. 1. The total water content transect used in this study from the GCE cloud model data at simulation time step $t = 240$ min.

II. CLOUD DATA AND RADIATIVE TRANSFER MODEL

Using nearby composite aircraft and radiosonde sounding data as initial environmental field, an oceanic tropical squall line was simulated by a realistic dynamical cloud model, the Goddard Cumulus Ensemble (GCE) model developed by Tao and Simpson [18]. The model domain is a $128 \times 128 \times 31$ grid with a horizontal resolution of 1.5 km and vertical resolution varying from 0.2 to 1.0 km from bottom to top (about 20 km). The GCE cloud model distinguishes five types of hydrometeors, namely cloud liquid water, rain water, cloud ice, snow, and graupel. Profiles of temperature and water vapor are also obtained along with profiles of the hydrometeors. Fig. 1 shows the total water content (total summed content of rain, cloud water, snow, cloud ice, and graupel) transect selected from the GCE cloud model data at simulation time step $t = 240$ min with one tilted cloud and one vertical cloud. The tilted structure of the cloud spans from $x = 75$ km to the left and the vertical structure of the cloud is around $x = 95$ km with a strong convective core. Above 5 km, the ice fraction of the total water content is about 98%. But, below that altitude, the liquid water prevails. Its contribution is about 93%.

A microwave radiative transfer model (RTM) [19] is used to calculate the microwave upwelling brightness temperatures between 89 and 190 GHz. The RTM considers the same five hydrometeor types as those obtained from the GCE cloud model data. All hydrometeors are treated as Mie spheres. The Maxwell-Garnett mixing theory [20] is used in the RTM for the ice and air mixtures of frozen hydrometeors to obtain the dielectric constant. The RTM does not employ a melting layers. The size distributions of rain, snow, and graupel are assumed to be exponentially distributed with

$$N(D) = N_0 \exp(-\lambda D), \quad (1)$$

where D is the diameter of particles, N_0 is the intercept parameter, and λ is the slope of the distribution depending on N_0 , the density of hydrometeor, and the hydrometeor water content. N_0 values used in this study are $2.2 \times 10^7 \text{ m}^{-4}$ for

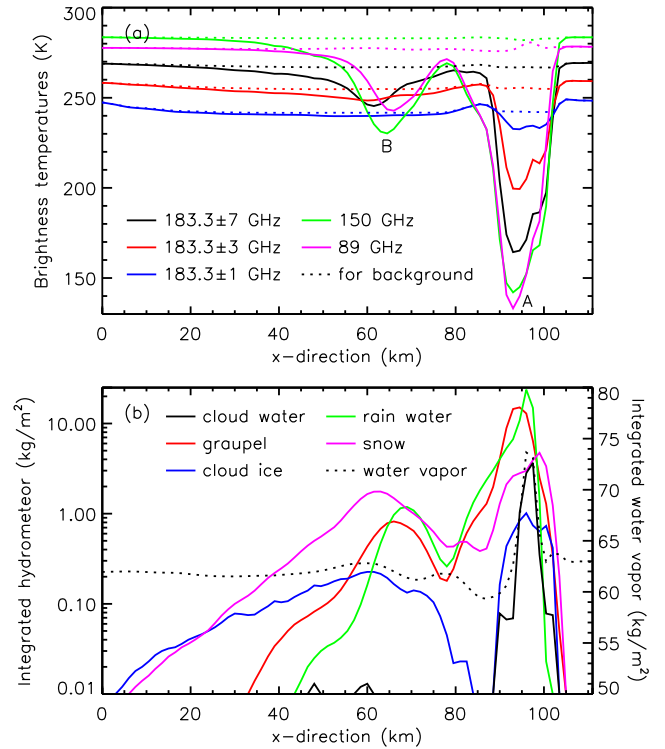


Fig. 2. (a) Brightness temperatures at 89–190 GHz simulated with the RTM. (b) Column-integrated cloud liquid water, rain water, cloud ice, snow, graupel, and water vapor for the transect in Fig. 1.

rain, 10^8 m^{-4} for snow, and $4 \times 10^6 \text{ m}^{-4}$ for graupel. The same N_0 values have been used in the TRMM version 6 of the 2A12 algorithm to retrieve hydrometeor profile (Haiyan Jiang, personal communication). The densities of rain, snow, and graupel are 1.0, 0.1, and 0.6 g cm^{-3} , respectively [2]. Wang *et al.* [11], [12] suggested that cloud ice in the upper portion of convection should be taken into account at high frequencies above 150 GHz. The distribution of cloud ice included in this version of the RTM is the one given by the fit to observed cloud ice distributions by Heymsfield and Platt [21]. The particle size of cloud water is gamma distributed according to Liou [22]. The densities of cloud ice and cloud liquid water are respectively 0.917 and 1.0 g cm^{-3} .

III. EFFECT OF CLOUD STRUCTURE ON MICROWAVE RADIANCES AT 89–190 GHz

Profiles of hydrometeors, temperature, and water vapor are used as inputs to the RTM to simulate brightness temperatures at 89–190 GHz. Only nadir observations are simulated in our study (Fig. 2(a)). The background brightness temperatures are simultaneously simulated from the same GCE cloud model data, without any hydrometeors. The GCE cloud model output, the column-integrated hydrometeors and water vapor are shown in Fig. 2(b).

In Fig. 2, at the vertical strong convection A, where the total ice water path (total summed path of cloud ice, snow, and graupel) is over 18 kg m^{-2} , and total liquid water path (total summed path of rain and cloud water) is over 20 kg m^{-2} , the 89 GHz simulations show the largest brightness temperature

depression defined as the difference between the simulated brightness temperature without (dotted lines in Fig. 2(a)) and including the hydrometeors (solid lines), then in sequence, 150, 183.3 ± 7 , 183.3 ± 3 , and 183.3 ± 1 GHz. For the three water vapor channels it is obvious that the channel farthest from absorption maximum at 183.3 GHz (i.e. 183.3 ± 7 GHz) has the largest depression. The brightness temperature at 183.3 ± 7 GHz is over 46 K lower than that at 183.3 ± 3 and over 92 K lower than that at 183.3 ± 1 GHz. This behavior is due to different weighting function at these channels [2]. The frequencies farther from the water vapor absorption center can see deeper into the clouds (e.g., 183.3 ± 7 GHz). Thus, they undergo larger influences from the hydrometeors in the low layers. The brightness temperature depressions of all frequencies between 89 and 190 GHz locate at the same point $x = 94.5$ km of the largest column-integrated total frozen hydrometeors.

Around the tilted structure cloud *B*, the brightness temperature depressions are much smaller than those for the strong convection and they have different features because of the tilted cloud structure. Relating the brightness temperature depressions to the column-integrated frozen hydrometeors, it is found that the places of largest brightness temperature depressions at 89 and 150 GHz correspond more to the peak of the column-integrated graupel amount and those around the water vapor channels correspond more to the peaks of the column-integrated snow and cloud ice amounts. Moreover, largest brightness temperature depressions at 89, 150, 183.3 ± 7 , 183.3 ± 3 , and 183.3 ± 1 GHz locate at different locations of $x = 66.0$, 64.5, 61.5, 60.0, and 54.0 km, respectively.

The total water content shown in Fig. 1 is investigated to understand the effect of the tilted cloud on brightness temperatures at 89–190 GHz. For the tilted cloud, the total water content above 5 km mainly stems from the ice water content, the highest total ice water content (over 0.6 g m^{-3}) being at $x = 66.0$ km. The channels at 89 and 150 GHz can see deeper than the water vapor channels and they have larger influence from the layer with larger total ice water content (below 7 km). So the locations of their largest brightness temperature depressions are on the right side of those for water vapor channels. The channels closer to water vapor absorption center are more sensitive to higher layers. Hence, 183.3 ± 1 GHz produces the largest brightness temperature depression first, then in sequence, 183.3 ± 3 and 183.3 ± 7 GHz. The variation of the locations of the maxima of the brightness temperature depression is clearly caused by the tilted distribution of total ice water content.

IV. ESTIMATION OF TILTED STRUCTURE FROM BRIGHTNESS TEMPERATURES

From the above description of the effects of one vertical cloud and one tilted cloud on brightness temperatures between 89 and 190 GHz, it is obvious that brightness temperature depressions are related not only to different sensitivities to vertical hydrometeors but also to the cloud structure. Different sensitivities to vertical hydrometeors result in different amounts of largest brightness temperature depressions. The

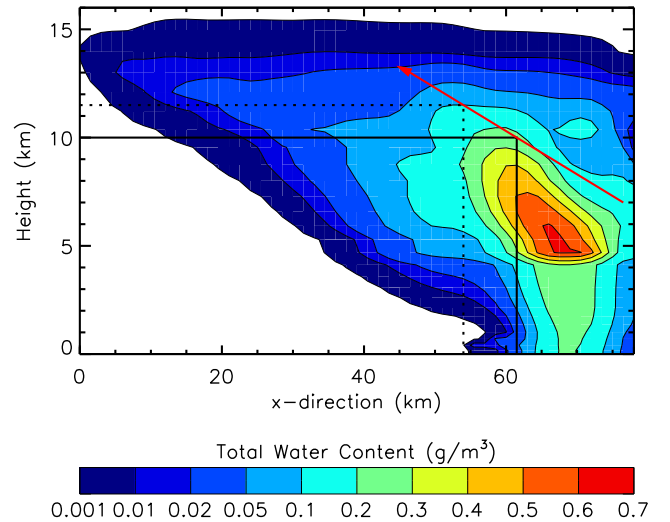


Fig. 3. Estimation of the canting angle of the tilted structure cloud. The horizontal lines are the altitudes of peaks of the weighting function at 183.3 ± 1 GHz (dotted one) and 183.3 ± 7 GHz (solid one), which are taken from the values from Fig. 6(B) of Burns *et al.* [2]. The vertical lines are the locations of the largest brightness temperature depressions at 183.3 ± 1 GHz (dotted one) and 183.3 ± 7 GHz (solid one). The tilted red line passing through the two points of intersection indicates the canting angle of the tilted structure cloud. The arrow in the red line shows the direction of the tilted structure cloud. Color contour is the distribution of total water content for the tilted structure cloud.

tilted structure of the cloud is the main cause for the mismatch of the locations of the maxima of the brightness temperature depressions at different frequencies. This mismatch reveals the difficulty to estimate the precipitation of clouds with tilted structures from microwave radiances at these frequencies. However, it provides a possibility to estimate the canting angle of the tilted structure of the cloud thereby obtain exacter locations of precipitation.

A method to estimate the canting angle is illustrated in Fig. 3. The water vapor channels around 183 GHz are chosen because of their lesser sensitivity to surface emission [10], [11]. An important prerequisite for estimating the canting angle of a tilted cloud is to know which layer (or altitude) the main contribution on brightness temperatures at the different frequencies comes from. In our study, the altitudes of the peaks of the weighting functions for the water vapor channels are taken from Burns *et al.* [2] (Fig. 6(B)), since the tilted cloud in our study has similar values of total ice water path and total water vapor as they have. The 183.3 ± 1 GHz channel always has a peak at a higher altitude than the 183.3 ± 7 GHz channel although the temperature weighting functions will change for different cloud hydrometeor profiles. The peak altitudes of the temperature weighting functions are at about 10.0 km for 183.3 ± 7 GHz and at 11.5 km for 183.3 ± 1 GHz. These altitudes indicate the main contribution layers on the brightness temperature depressions at 183.3 ± 7 and 183.3 ± 1 GHz respectively in the vertical direction of cloud. The different horizontal locations of the largest brightness temperature depressions indicate the place of the main contributions on the brightness temperature depressions in the horizontal direction. Therefore, the canting angle of

the tilted cloud can be estimated from the slope of the line passing through the two points of intersection created by corresponding peak altitudes of the weighting functions and the locations of the largest brightness temperature depressions at 183.3 ± 1 and 183.3 ± 7 GHz, which is shown by the red line in Fig. 3. Note that the retrieved canting angle depends only on the difference in the peak altitudes of the weighting functions, not on the maximum values themselves. The tilt direction of the tilted cloud can be derived by the relative location of the largest brightness temperature depression at 183.3 ± 1 GHz with respect to the location of the largest brightness temperature depression at 183.3 ± 7 GHz. It is obvious that the estimated canting angle (the red line) is in agreement with the canting angle of the tilted cloud, and the derived tilt direction is in agreement with the actual tilt direction of the cloud.

V. APPLICATION TO AN AIRCRAFT CASE

This method is applied to a tilted storm observed from the NASA ER-2 aircraft flying at about 20 km altitude along a straight track from 1632:05 to 1643:11 UTC (from $(79.60^\circ\text{W}, 33.27^\circ\text{N})$ to $(76.15^\circ\text{W}, 33.21^\circ\text{N})$) on 26 August 1998 during the Convection And Moisture EXperiment (CAMEX)-3. Fig. 4 shows the collocated simultaneous down-looking observations at nadir including the microwave brightness temperatures at the three water vapor channels around 183.3 GHz from the Millimeter-wave Imaging Radiometer (MIR), the reflectivity from the ER-2 Doppler radar (EDOP), and the estimated canting angle and tilt direction of the storm.

The EDOP radar sampling at 9.6 GHz with a vertical resolution of 37.5 m [23] provides direct information on tilted cloud structure (Fig. 4(b)). Again, as in the above synthetic case, the brightness temperatures at the three water vapor channels around 183.3 GHz have different locations of their depression maxima (Fig. 4(a)) because of the tilted cloud structure and the different sensitivities to vertical hydrometeors in the cloud. The peak altitudes of the temperature weighting function at about 10.0 km for 183.3 ± 7 GHz and 11.5 km for 183.3 ± 1 GHz are also used in this case. Then, the canting angle and tilt direction of the cloud are estimated (read arrow in Fig. 4(b)). The results agree well with the EDOP radar observation. With respect to the simulated case, the benefit of using the canting angle to estimate the surface precipitation location is weaker for the aircraft case. This is due to the lower spatial correlation of frozen hydrometeor contents in the observed cloud than in those from the model simulations. However, there is still a slight displacement present between the brightness temperature depression minimum at 183.3 ± 1 GHz and the surface precipitation core. This reveals that estimating the canting angle can be used to improve the estimation of the surface precipitation location using the microwave frequencies sensitive to high altitudes (e.g., 183.3 ± 1 GHz) [14].

In order to explore this possibility, five more cases of tilted deep convective clouds from the CAMEX-3 campaign were analyzed (not shown here) in presentations similar to Fig. 4. In three of the six cases in total, it was possible to detect the canting angle correctly as verified visually from the EDOP

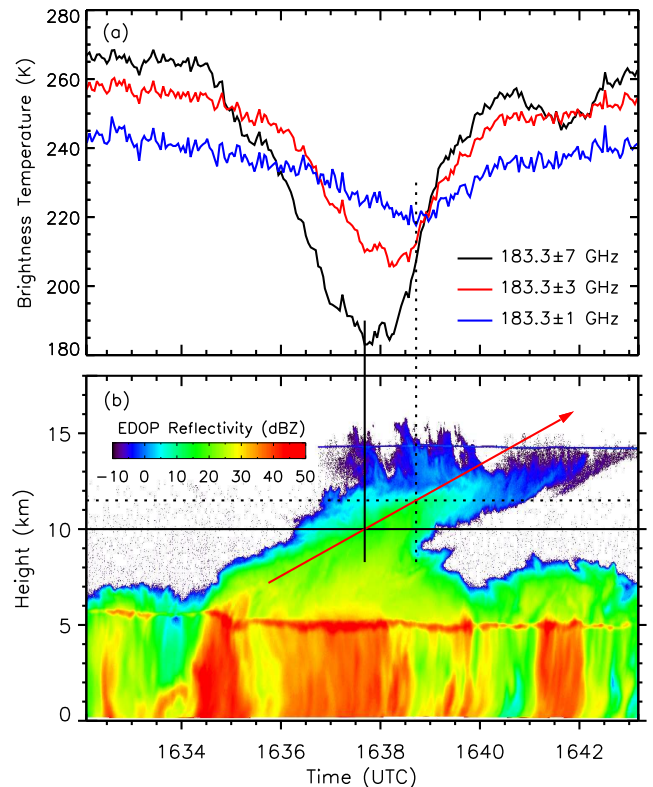


Fig. 4. Time series of MIR and EDOP data along the flight track from 1632:05 to 1643:11 UTC on 26 August 1998 during CAMEX-3 (1 min \approx 13 km). (a) microwave brightness temperatures at the three water vapor channels around 183.3 GHz observed from MIR, (b) EDOP reflectivity cross sections. The tilted red line indicates the canting angle of the tilted structure cloud. The arrow in the red line shows the direction of the tilted structure cloud. The horizontal dotted and solid lines are the altitudes of peaks of the weighting function at 183.3 ± 1 and 183.3 ± 7 GHz, respectively. The vertical dotted and solid lines are the locations of the largest brightness temperature depressions at 183.3 ± 1 and 183.3 ± 7 GHz, respectively.

data. The procedure gives information about the tilting in the high region of the weighting functions of the two involved channels, i.e. between 10 and 11 km. Therefore, only if the tilt is vertically constant from the melting layer (indicated in Fig. 4b as a horizontal red band between 5 and 6 km altitude) to the cloud top, this information may be used to estimate the precipitation location (Fig. 4). However, if the tilt is not vertically constant, but bended, we would need more information about the cloud shear structure between 5 and 10 km altitude in order to locate the precipitation (one case not shown). In the three failing cases, the separation of the brightness temperature minima of the two involved channels was too low (less than 3 km) or zero.

VI. CONCLUSION

We have investigated the effects of one vertical cloud and one tilted cloud on brightness temperatures at the frequencies between 89 and 190 GHz using a microwave radiative transfer model with cloud resolving model simulations as they would be observed from satellite or aircraft microwave radiometric sensors in nadir direction. We have found a method to estimate the canting angle and tilt direction of tilted clouds using water vapor channels at 183.3 ± 1 and 183.3 ± 7 GHz. The estimated

canting angle and tilt direction are in agreement with the actual canting angle of and tilt direction of the tilted structure in the cloud model simulations. The method is applied to a tilted storm observed by simultaneous aircraft microwave measurements at the water vapor channels and with radar. The results agree well with the radar observations. At the same time, this method could provide a possibility to estimate the displacement of the cloud vertical structure to estimate the accurate location of surface rainfall for precipitating retrieval methods based on the ice scattering above surface rainfall using the microwave frequencies sensitive to high altitudes. Realistic cloud structures are generally weaker, lower, less spatially correlated, and exhibiting smaller contents of frozen hydrometeors than the simulated precipitation structures. This can cause that the displacement between the positions of local minima of the 183.3 ± 1 and 183.3 ± 7 GHz brightness temperatures may not be as large as in the cases we investigated, making it more difficult to use the method for real clouds. Also, this methodology is applicable to airborne observations rather than to satellite observations since satellite instruments, i.e. AMSU-B, have quite coarse resolutions (especially at the edges) which may obscure the displacement between the positions of local minima of the brightness temperatures at the two frequencies.

ACKNOWLEDGMENT

We thank J. Wang and G. Skofronick-Jackson for providing us with GCE cloud model data; C. Kummerow for providing and helping us with his RTM codes; J. Wang and P. Racette for production of the MIR data; G. Heymsfield and N. Ferreira for the production of the EDOP data; H. Jiang for helping with the parameters of particle size distribution; the Distributed Active Archive Center (DAAC) at the Goddard Space Flight Center, which archives and distributes the MIR and EDOP data under sponsorship of NASA's Earth Science Enterprise. We also thank constructive comments and suggestions from the reviewers. G. Hong is grateful to the Gottlieb Daimler- und Karl Benz- Foundation and University of Bremen for their support.

REFERENCES

- [1] P. W. Rosenkranz, "Retrieval of temperature and moisture profiles from AMSU-A and AMSU-B measurements," *IEEE Trans. Geosci. Remote Sens.*, vol. 39, no. 11, pp. 2429–2435, 2001.
- [2] B. A. Burns, X. Wu, and G. R. Diak, "Effects of precipitation and cloud ice on brightness temperatures in AMSU moisture channels," *IEEE Trans. Geosci. Remote Sens.*, vol. 35, no. 6, pp. 1429–1437, 1997.
- [3] T. J. Greenwald, and S. A. Christopher, "Effect of cold clouds on satellite measurements near 183 GHz," *J. Geophys. Res.*, vol. 107, no. D13, 2002.
- [4] J. R. Eyre, "The information content of data from operational satellite sounding systems: A simulation study," *Q. J. R. Meteorol. Soc.*, vol. 116, pp. 401–434, 1990.
- [5] G. Liu, and J. A. Curry, "Tropical ice water amount and its relations to other atmospheric hydrological parameters as inferred from satellite data," *J. Appl. Meteorol.*, vol. 38, pp. 1182–1194, 1999.
- [6] L. Zhao, and F. Weng, "Retrieval of ice cloud parameters using the Advanced Microwave Sounding Unit," *J. Appl. Meteorol.*, vol. 41, pp. 384–395, 2002.
- [7] F. Weng, L. Zhao, R. R. Ferraro, G. Poe, X. Li, and N. C. Grody, "Advanced microwave sounding unit cloud and precipitation algorithms," *Radio Sci.*, vol. 38, no. 4, 2003.
- [8] B. M. Muller, H. E. Fuelberg, and X. Xiang, "Simulations of the effects of water vapor, cloud liquid water, and ice on AMSU moisture channel brightness temperatures," *J. Appl. Meteorol.*, vol. 33, pp. 1133–1154, 1994.
- [9] G. M. Skofronick-Jackson, A. J. Gasiewski, and J. R. Wang, "Influence of microphysical cloud parameterizations on microwave brightness temperatures," *IEEE Trans. Geosci. Remote Sens.*, vol. 40, pp. 187–196, 2002.
- [10] R. Bennartz, and P. Bauer, "Sensitivity of microwave radiances at 85–183 GHz to precipitating ice particles," *Radio Sci.*, vol. 38, no. 4, 2003.
- [11] J. R. Wang, J. Zhan, and P. Racette, "Storm-associated microwave radiometric signatures in the frequency range of 90–220 GHz," *J. Atmos. Ocean Technol.*, vol. 14, pp. 13–31, 1997.
- [12] J. R. Wang, J. Zhan, and P. Racette, "Multiple aircraft microwave observations of storms over the western Pacific Ocean," *Radio Sci.*, vol. 33, pp. 351–368, 1998.
- [13] G. M. Skofronick-Jackson, and J. R. Wang, "The estimation of hydrometeor profiles from wideband microwave observations," *J. Appl. Meteorol.*, vol. 39, pp. 1645–1657, 2000.
- [14] D. H. Staelin, and F. W. Chen, "Precipitation observations near 54 and 183 GHz using the NOAA-15 satellite," *IEEE Trans. Geosci. Remote Sens.*, vol. 38, pp. 2322–2332, 2000.
- [15] M. A. LeMone, G. M. Barnes, E. J. Szoke, and E. J. Zipser, "The tilt of leading edge of mesoscale tropical convective lines," *Mon. Wea. Rev.*, vol. 112, pp. 510–519, 1984.
- [16] G. Mcgaughey, E. J. Zipser, R. W. Spencer, and R. E. Hood, "High-resolution passive microwave observations of convective systems over the tropical pacific ocean," *J. Appl. Meteorol.*, vol. 35, pp. 1921–1947, 1996.
- [17] Y. Hong, J. L. Haferman, W. S. Olson, and C. D. Kummerow, "Microwave brightness temperatures from titled convective systems," *J. Appl. Meteorol.*, vol. 39, pp. 983–998, 2000.
- [18] W.-K. Tao, and J. Simpson, "Goddard cumulus ensemble model. Part I: Model description," *Terr. Atmos. Oceanic Sci.*, vol. 4, pp. 35–72, 1993.
- [19] C. Kummerow, W. S. Olson, and L. Giglio, "A simplified scheme for obtaining precipitation and vertical hydrometeor profiles from passive microwave sensors," *IEEE Trans. Geosci. Remote Sens.*, vol. 34, pp. 1213–1232, 1996.
- [20] C. F. Bohren, and L. J. Battan, "Radar backscattering by inhomogeneous precipitation particles," *J. Atmos. Sci.*, vol. 37, pp. 1821–1827, 1980.
- [21] A. J. Heymsfield, and C. M. R. Platt, "A parameterization of the particle size spectrum of ice clouds in terms of the ambient temperature and the ice water content," *J. Atmos. Sci.*, vol. 41, pp. 846–855, 1984.
- [22] K. N. Liou, *Radiation and cloud processes in atmosphere: Theory, Observation, and Modeling*, Oxford: Oxford Univ. Press, 487 pp., 1992.
- [23] G. M. Heymsfield, J. M. Shepherd, S. W. Bidwell, W. C. Boncyk, I. J. Caylor, S. Ameen, and W. S. Olson, "Structure of Florida thunderstorms using high-altitude aircraft radiometer and radar observations," *J. Appl. Meteorol.*, vol. 35, 1736–1762, 1996.